

A METHOD FOR DIMENSIONALLY ADAPTIVE SPARSE TRIGONOMETRIC INTERPOLATION OF PERIODIC FUNCTIONS*

ZACK MORROW[†] AND MIROSLAV STOYANOV[‡]

Abstract. We present a method for dimensionally adaptive sparse trigonometric interpolation of multidimensional periodic functions belonging to a smoothness class of finite order. This method is useful for problems where periodicity must be preserved and the precise anisotropy is not known *a priori*. The motivating application behind this work is the adaptive approximation of a multi-input model for a molecular potential energy surface (PES) where each input represents an angle of rotation. Our method is based on an anisotropic quasi-optimal estimate for the decay rate of the Fourier coefficients of the model; a least-squares fit to the coefficients of the interpolant is used to estimate the anisotropy. Thus, our adaptive approximation strategy begins with a coarse isotropic interpolant, which is gradually refined using the estimated anisotropic rates. The procedure takes several iterations where ever-more accurate interpolants are used to generate ever-improving anisotropy rates. We present several numerical examples of our algorithm where the adaptives procedure successfully recovers the theoretical “best” convergence rate, including an application to a periodic PES approximation. An open-source implementation of our algorithm resides in the Tasmanian UQ library developed at Oak Ridge National Laboratory.

Key words. Sparse interpolation, trigonometric interpolation, adaptive refinement, periodicity-preserving approximation

AMS subject classifications. 65D05, 65D15, 65T40, 92E10

1. Introduction. Consider the approximation of a multidimensional function (i.e., model) $f : \mathbb{T}^d \rightarrow \mathbb{R}$, where $\mathbb{T} = [0, 1]$ represents a torus and f is both differentiable and periodic up to a given finite order. The order of differentiability and periodicity can vary with each dimension. The main challenge of approximating a computationally expensive model in a multidimensional (multi-input) setting is the rapid growth of required model simulations per dimension d , a phenomenon that is known as the *curse of dimensionality* [3].

Various techniques exist to mitigate, or in rare cases eliminate, the curse of dimensionality. Global and derivative-based sensitivity analysis enables the identification of noninfluential parameters, thereby reducing the effective dimensionality of the problem to include only inputs and directions that contribute towards the model output variability [15, 52]. Other methods seek to reduce the complexity of the target function f by approximating it with functions that are in some sense “simpler.” This could be done, for instance, by projection onto or interpolation within a polynomial or trigonometric function space, both of which use samples, i.e., the values of the target function for a set of independent inputs. Sampling methods are attractive due to their non-intrusive nature, which can be easily wrapped around existing third-party or black-box models.

Let $\{\varphi_\nu\}_{\nu \in \mathbb{N}^d}$ be an orthonormal basis for the Hilbert space where f resides (e.g., L^2), and let $\Lambda \subset \mathbb{N}^d$ be finite.¹ A well-known result states that orthogonal projection

*Submitted to the editors on August 23, 2019.

[†]Department of Mathematics, North Carolina State University, Raleigh, NC 27695 (zbmorrow@ncsu.edu).

[‡]Corresponding author. Computational and Applied Mathematics Group, Oak Ridge National Laboratory, Oak Ridge, TN 37830 (stoyanovmk@ornl.gov).

¹This paper adopts the convention $\mathbb{N} = \{0, 1, 2, \dots\}$.

of f onto $\text{span}\{\varphi_\nu\}_{\nu \in \Lambda}$ yields the optimal L^2 error [26, p. 352]; that is,

$$(1.1) \quad c_\nu = \langle f, \varphi_\nu(\mathbf{x}) \rangle \Rightarrow \left\| f - \sum_{\nu \in \Lambda} c_\nu \varphi_\nu \right\| = \min_{g \in \text{span}\{\varphi_\nu\}_{\nu \in \Lambda}} \|f - g\|.$$

Here, $\{c_\nu\}_{\nu \in \Lambda}$ are the optimal expansion coefficients, and $\langle \cdot, \cdot \rangle$ and $\|\cdot\|$ denote the Hilbert space inner product and norm respectively. In general, the integral coefficients in (1.1) must be evaluated numerically, e.g., with a multidimensional numerical quadrature. Thus, projection methods often come at a high computational cost due to the large number of function samples necessary to approximate c_ν to a sufficient accuracy [2, 53, 54] which can far exceed the number of basis functions. In contrast, interpolation methods require a single sample per basis function, although the resulting approximation is not Hilbert-optimal. The interpolation error is bounded by the best projection error multiplied by a penalty term called the *Lebesgue constant*, but the degradation in accuracy is usually offset by the reduction in complexity. In particular, sparse interpolation methods [46], which are of focus of this paper, often have better overall convergence rate with respect to the number of samples [53].

To further improve the convergence rate of sparse-grid interpolation, many methods gauge the approximation error in order to determine the most important directions and spatial locations in which to sample next. Such procedures are known as *adaptive refinement*, and the overall goal is to select the samples that would result in the fastest convergence rate. Bungartz and Griebel formulated this procedure as a knapsack problem in which they maximize the added accuracy subject to cost constraints at each refinement iteration until the interpolation error reaches a desired accuracy [4].

Recent developments in quasi-optimal approximation utilize theoretical upper bounds on the decay rates of the expansion coefficients c_ν (rather than the exact c_ν themselves) in order to refine the approximation iteratively. For a fixed number of terms M in the expansion, such approaches often result in a tighter error bound. Much of the previous work on quasi-optimal approximation is done in the context of Legendre expansions of holomorphic functions. Authors have deployed quasi-optimal approximation in the context of projection [55] and sparse-grid interpolation [34, 53].

In contrast to previous work, this paper considers periodic functions, i.e., $f \in L^2(\mathbb{T}^d)$, such that, for each $1 \leq k \leq d$,

$$\left\| \frac{\partial^m f}{\partial x_k^m} \right\|_{L^2(\mathbb{T}^d)} < \infty, \quad \frac{\partial^m f(0)}{\partial x_k^m} = \frac{\partial^m f(1)}{\partial x_k^m}, \quad \forall m \in \{0, 1, \dots, n_k\}$$

where n_k is the order of periodicity in dimension k . The torus domain and the periodic boundary conditions lead to the natural choice of basis of trigonometric polynomials [18]. In this paper, we present a multidimensional sparse-grid trigonometric-basis adaptive interpolation technique for periodic functions with different degrees of smoothness in each direction. The smoothness affects the convergence rate, so we will use anisotropic grids with rates of anisotropy estimated using a least-squares fitting of the Fourier coefficients of the interpolant, which is similar to previous work in the context of total-degree, polynomial-based interpolation for holomorphic functions [53].

The rest of the paper is organized as follows. In [section 2](#), we derive the trigonometric quasi-optimal approximation space using theoretical bounds on the decay rates of the Fourier coefficients. In [section 3](#), we describe anisotropic sparse trigonometric interpolation and present our adaptive refinement algorithm. In [section 4](#), we provide several numerical examples using both simple polynomials with known degrees

of periodicity and the PES model. Finally, [section 5](#) offers a brief summary of our results.

2. Quasi-optimal function space. First, we consider the space of multidimensional periodic functions. Using upper bounds on the Fourier coefficients, we derive the quasi-optimal approximation space in the context of projection. From projection we proceed to interpolation and derive the quasi-optimal interpolation space. We conclude by discussing how to estimate the anisotropic coefficients of the target function *on-the-fly*.

Let $H^n(\mathbb{T}) \subset C^n(\mathbb{T})$, with $n \geq 0$, denote the space of n -times continuously differentiable functions $f : \mathbb{T} \rightarrow \mathbb{R}$ such that f has n periodic derivatives and $f^{(n+1)}$ is piece-wise continuous with only isolated jump discontinuities. In the d -dimensional case, for $\mathbf{n} = (n_1, n_2, \dots, n_d)$, we define

$$H^{\mathbf{n}}(\mathbb{T}^d) = H^{n_1}(\mathbb{T}) \otimes \dots \otimes H^{n_d}(\mathbb{T})$$

so that for any $f \in H^{\mathbf{n}}(\mathbb{T}^d)$, $1 \leq k \leq d$, and $(x_1, x_2, \dots, x_d) \in \mathbb{T}^d$

$$f(x_1, \dots, x_{k-1}, x, x_{k+1}, \dots, x_d) \in H^{n_k},$$

i.e., restricting f to a single dimension yields a function in $H^{n_k}(\mathbb{T})$. Here, without loss of generality, we take the canonical torus $\mathbb{T}^d = [0, 1]^d$ since any arbitrary torus $\Gamma = \bigotimes_{k=1}^d [a_k, b_k]$ can be translated to \mathbb{T}^d with a simple affine transformation.

The coefficients of the Fourier expansion of $f \in H^{\mathbf{n}}$ are defined as

$$(2.1) \quad c_{\mathbf{j}}(f) = \int_{\mathbb{T}^d} \exp(-2\pi i \mathbf{j} \cdot \mathbf{x}) f(\mathbf{x}) d\mathbf{x}, \quad \mathbf{j} \in \mathbb{Z}^d,$$

with $i^2 = -1$ and $\mathbf{j} \cdot \mathbf{x} = \sum_{k=1}^d j_k x_k$. In a single dimensional context, using Theorems 1.6, 4.4, and 4.5 from [\[22, pp. 4, 25\]](#) and trivial re-indexing, we obtain

$$(2.2) \quad |c_j(f)| \leq \frac{C}{(1 + |j|)^{n+2}}, \quad j \in \mathbb{Z}, \quad f \in H^n(\mathbb{T}),$$

for some constant $C > 0$. Furthermore, since $f^{(n+1)}$ has jump discontinuities, the bound in [\(2.2\)](#) is sharp [\[11, p. 200\]](#). In a multidimensional context, using the tensor-product structure of the space, we have

$$(2.3) \quad |c_{\mathbf{j}}(f)| \leq \frac{C}{\prod_{k=1}^d (1 + |j_k|)^{n_k+2}}, \quad \mathbf{j} \in \mathbb{Z}^d, \quad f \in H^{\mathbf{n}}(\mathbb{T}^d).$$

Function spaces like this have appeared in the literature as weighted Korobov spaces. In an early work on sparse trigonometric interpolation, Hallatschek [\[14\]](#) considered the Korobov space

$$(2.4) \quad E_a^d = \left\{ f \in L^2([0, 1]^d) : \exists C > 0 \text{ s.t. } \forall \mathbf{j} \in \mathbb{Z}^d, |c_{\mathbf{j}}(f)| \leq C \prod_{k=1}^d (1 + |j_k|)^{-a} \right\}$$

where $a > 1$ is a smoothness parameter. In general, a may take on any real value greater than one, but integer values have an interpretation in terms of the order of differentiability [\[39\]](#). One may directly connect $a \in \{2, 3, \dots\}$ back to $H^{\mathbf{n}}(\mathbb{T}^d)$ and [\(2.3\)](#) by taking $\mathbf{n} = (a - 2, \dots, a - 2)$. However, there is precedent in the

literature for our consideration of anisotropic, rather than isotropic, approximations for functions obeying (2.3). Authors have recently studied tractability questions in anisotropic Korobov spaces [28, 38, 39] in addition to approximation in anisotropic Sobolev and Besov spaces [45]. There is also a long tradition of dimensionally and spatially adaptive refinement within the context of sparse-grid interpolation with a piece-wise or Lagrange polynomial basis, e.g. [4, 13, 19, 20, 21, 23, 24, 31, 33, 34, 35, 40, 41, 49, 51, 53]. Our method differs from previous work by using trigonometric basis functions rather than polynomials and by estimating the anisotropy using a fit to a sharp bound on the decay rate of Fourier coefficients (2.3); see subsection 2.3.

2.1. Quasi-optimal projection space. Consider the projection of $f \in H^n(\mathbb{T}^d)$ onto a subspace of real trigonometric polynomials defined by $\Lambda(L) \subset \mathbb{N}^d$:

$$(2.5) \quad \mathbb{P}_{\Lambda(L)} = \bigcup_{\nu \in \Lambda(L)} \mathbb{P}_\nu = \bigcup_{\nu \in \Lambda(L)} \bigotimes_{k=1}^d \mathbb{P}_{\nu_k}$$

where

$$(2.6) \quad \mathbb{P}_n = \text{span}\{1, \cos(2\pi x), \dots, \cos(2\pi n x), \sin(2\pi x), \dots, \sin(2\pi n x)\}.$$

For convenience, we have slightly different definitions based on whether the subscript is a scalar or a set. Here, we assume $\Lambda(L)$ is a finite lower set,² and the parameter L discretizes the multi-index space into levels.

Let $f_{\Lambda(L)}$ be the best approximation to f in $\mathbb{P}_{\Lambda(L)}$ in the $L^2(\mathbb{T}^d)$ sense, i.e., $f_{\Lambda(L)}$ is defined from the orthogonal decomposition of f in terms of trigonometric polynomials $T_\nu(\mathbf{x})$:

$$f(\mathbf{x}) = \sum_{\nu \in \mathbb{N}^d} c_\nu T_\nu(\mathbf{x}), \quad f_{\Lambda(L)}(\mathbf{x}) = \sum_{\nu \in \Lambda(L)} c_\nu T_\nu(\mathbf{x}),$$

which is the familiar Fourier series. It follows that the best M -term approximation space for projection is associated with the M largest Fourier coefficients of f . Therefore, taking the upper bound in (2.3) with $\alpha_k = n_k + 2$, we obtain the quasi-optimal space

$$(2.7) \quad \Lambda^\alpha(L) = \{\mathbf{i} \in \mathbb{N}^d : (\mathbf{i} + \mathbf{1})^\alpha \leq L\}, \quad \text{where } \nu^\alpha = \prod_{k=1}^d \nu_k^{\alpha_k}.$$

Note that the structure of the multi-indexes corresponds to a hyperbolic space, which is in contrast to the total-degree space, commonly used for sparse grids [1, 14, 36, 37]:

$$(2.8) \quad \Lambda_{TD}^\alpha(L) = \{\mathbf{i} \in \mathbb{N}^d : \alpha \cdot \mathbf{i} \leq L\}.$$

2.2. Quasi-optimal interpolation. Projection yields the optimal L^2 error, but computing c_ν to a sufficient accuracy involves a number of function samples typically much larger than the size of the basis $\mathbb{P}_{\Lambda(L)}$. In contrast, interpolation requires exactly the same number of samples as basis functions at the cost of slight reduction of accuracy. Thus, in many practical situations, interpolation results in a better overall convergence rate.

²A set Λ is called *lower* if $\nu \in \Lambda$ implies $\{\mathbf{i} \in \mathbb{N}^d : \mathbf{i} \leq \nu\} \subset \Lambda$, where $\mathbf{i} \leq \nu$ if and only if $i_k \leq \nu_k$ for each $1 \leq k \leq d$.

In this subsection, we consider $f_{\Lambda(L)}$ as an interpolatory (rather than projective) approximation to f . Specifically, $f_{\Lambda(L)}$ is obtained from applying the interpolation operator $I_{\Lambda(L)}$ to f , where the operator is exact for all functions in $\mathbb{P}_{\Lambda(L)}$. Following classical results in interpolation (e.g., [10]), for all $T \in \mathbb{P}_{\Lambda(L)}$ we have

$$\begin{aligned} \|f - f_{\Lambda(L)}\|_{\infty} &= \|f - T + T - f_{\Lambda(L)}\|_{\infty} \\ &= \|f - T + I_{\Lambda(L)}[T - f]\|_{\infty} \\ &\leq \|f - T\|_{\infty} + \|I_{\Lambda(L)}\| \|f - T\|_{\infty}, \end{aligned}$$

where

$$(2.9) \quad \|I_{\Lambda(L)}\| = \sup_{\|u\|_{\infty}=1} \|I_{\Lambda(L)}[u]\|_{\infty}$$

and $\|\cdot\|_{\infty}$ is the L^{∞} norm on \mathbb{T}^d . Taking the infimum over all $T \in \mathbb{P}_{\Lambda(L)}$, we obtain

$$(2.10) \quad \|f - f_{\Lambda(L)}\|_{\infty} \leq (1 + \mathbb{L}_{\Lambda(L)}) \inf_{T \in \mathbb{P}_{\Lambda(L)}} \|f - T\|_{\infty},$$

where $\mathbb{L}_{\Lambda(L)}$ is norm of the interpolation operator, commonly called the *Lebesgue constant*. Note that in our context the word *constant* is a misnomer since it strongly depends on the approximation space $\Lambda(L)$ and the specific choice of samples; a detailed discussion is included in [section 3](#). Here we observe that

$$(2.11) \quad \inf_{T \in \mathbb{P}_{\Lambda(L)}} \|f - T\|_{\infty} \leq \left\| f - \sum_{\nu \in \Lambda(L)} c_{\nu} T_{\nu} \right\|_{\infty}$$

where the coefficients c_{ν} come from the best L^2 approximation. We can chain together (2.10)-(2.11) and note that the only difference from the optimal L^2 approximation comes from using the L^{∞} rather than L^2 norm. We end up deriving the same quasi-optimal space as in Equation (2.7) by heuristically approximating interpolation error as a combination of L^2 projection error and the Lebesgue constant. Other papers have included more parameters in the quasi-optimal interpolation space in order to incorporate the effects of the Lebesgue constant [53], but this is not necessary in our context; see [subsection 3.3](#).

2.3. Estimating anisotropy. The specific values of the entries in the anisotropy vector α , while critical for constructing a quasi-optimal approximation, are seldom known *a priori*. In this section, we describe a method for estimating the anisotropy from an already constructed approximation $f_{\Lambda(L)}$ for some lower set $\Lambda(L)$. By definition, since $f_{\Lambda(L)} \in \mathbb{P}_{\Lambda(L)}$

$$f_{\Lambda(L)}(\mathbf{x}) = \sum_{\nu \in \Lambda(L)} \hat{c}_{\nu} T_{\nu}(\mathbf{x})$$

where \hat{c}_{ν} are either the projection coefficients from [subsection 2.1](#) or a corresponding set of interpolation weights. Often times, the \hat{c}_{ν} are explicitly computed as part of the respective projection or interpolation procedure and hence available at no additional cost. If the estimate in (2.3) bounds the decay of \hat{c}_{ν} sharply, then

$$(2.12) \quad |\hat{c}_{\nu}| \approx \tilde{C} \prod_{k=1}^d (1 + |\nu_k|)^{-\alpha_k}$$

and the rates can be inferred from only two samples in each direction. However, in practice, the estimate is only an upper bound and the individual coefficients can vary, which gives an effect similar to noise. Thus, in order to cancel the noise, we take more samples in each direction and solve for the effective rates of decay from an over-determined set of equations. Taking the log of both sides and changing signs, we obtain

$$(2.13) \quad -\log(|\hat{c}_\nu|) \approx -C + \boldsymbol{\alpha} \cdot \log(\boldsymbol{\nu} + \mathbf{1}), \quad \forall \boldsymbol{\nu} \in \Lambda(L).$$

for some constant C (different from the constant in (2.3)), where

$$\log(\mathbf{i}) = \bigotimes_{k=1}^d \log(i_k).$$

To average out the effects of the “noise,” we take the least-squares solution, i.e., the solution that minimizes the ℓ^2 norm

$$(2.14) \quad \min_{\boldsymbol{\alpha}, C} \frac{1}{2} \sum_{\boldsymbol{\nu} \in \Lambda(L)} (C + \boldsymbol{\alpha} \cdot \log(\boldsymbol{\nu} + \mathbf{1}) + \log(|\hat{c}_\nu|))^2.$$

which can be written in a matrix form

$$(2.15) \quad \min_{\mathbf{v}} \frac{1}{2} \|\mathbf{A}\mathbf{v} - \mathbf{b}\|_2,$$

where the rows of \mathbf{A} have the form $(1, \log(v_1 + 1), \log(v_2 + 1), \dots, \log(v_d + 1))$, the solution is $\mathbf{v} = (C, \alpha_1, \dots, \alpha_d)^T$, and \mathbf{b} holds the corresponding entries of $\log(\hat{c}_\nu)$. Equation (2.15) admits a unique solution so long as \mathbf{A} has full column rank, i.e., so long as we have at least two coefficients in each direction to estimate the corresponding decay rate. However, the accuracy of the estimated rates is also heavily dependent on the condition number of \mathbf{A} , and since (2.12) is only an approximation, more than a couple of coefficients are required. Also note that the constant C does not enter into the estimate of $\boldsymbol{\alpha}$ except as a dummy variable and a regularizer within the least-squares problem.

3. Sparse trigonometric interpolation. In this section, we describe a sparse-grid approach for constructing an interpolant $f_{\Lambda(L)} \in \mathbb{P}_{\Lambda(L)}$ based on the values of f at a set of nodes $\mathbf{x}_1, \dots, \mathbf{x}_M \in \mathbb{T}^d$. Here, we make no optimality assumptions about $\Lambda(L)$; we only assume that $\Lambda(L)$ is a lower set. After discussing the sparse interpolation algorithm, we examine the Lebesgue constant in the sparse-grid case. We conclude by coupling the anisotropy-estimation procedure of subsection 2.3 with a general sparse trigonometric interpolation algorithm in order to produce a dimensionally adaptive interpolant.

3.1. One dimension and full-tensor. To begin, we define the one dimensional m -point trigonometric interpolation rule. The nodes and (global) basis functions are

$$(3.1) \quad x_j = \frac{j}{m}, \quad \phi_j(x) = \exp(2\pi i \sigma(j) x), \quad j = 0, 1, \dots, m-1,$$

Because approximations using cosines and sines up to mode n require complex exponentials with powers ranging between $-n \leq j \leq n$ [48], we define

$$(3.2) \quad \sigma(j) = \begin{cases} -j/2, & j \text{ even} \\ (j+1)/2, & j \text{ odd} \end{cases}.$$

Remark 3.1. One-dimensional trigonometric interpolation with even numbers of points has precedent in the literature [8, 48]. Indeed, much work with Fourier transforms on sparse grids uses 2^l points at each level [12, 14] since powers of 2 are highly amenable to fast Fourier transforms. However, for the purposes of interpolation, an even number of points $m = 2n$ exactly reproduces all modes up to $n - 1$ due to the missing conjugate exponent for mode n . Put differently, there is an additional basis function for $m = 2n$ vs. $m = 2n - 1$ without a general increase in exactness in terms of both sines and cosines. Therefore, we use an odd number of interpolation nodes, which means \mathcal{U}^m is exact up to mode $(m - 1)/2$.

To resolve all sine and cosine modes up to n , it is necessary and sufficient to take $m = 2n + 1$ points [48]. The interpolation operator is

$$(3.3) \quad \mathcal{U}^m : C^0(\mathbb{T}) \rightarrow \mathbb{P}_{(m-1)/2}, \quad \mathcal{U}^m[f](x) = \sum_{j=0}^{m-1} \Re[\hat{c}_j \phi_j(x)],$$

where \hat{c}_j are the interpolation coefficients and \mathbb{P}_n is defined by (2.6). When we evaluate the interpolant in (3.3), we take only the real part; expressing the basis functions as complex exponentials is done for clarity of presentation. To impose the interpolation conditions

$$\mathcal{U}^m[f](x_j) = f(x_j), \quad j = 0, 1, \dots, m - 1,$$

it has been shown [12, 14, 48] that

$$(3.4) \quad \hat{c}_j = \frac{1}{m} \sum_{p=0}^{m-1} f(x_p) [\phi_j(x_p)]^*$$

where $[\cdot]^*$ denotes complex conjugation. With some algebra work, it becomes apparent that (3.4) is a normalized and re-indexed discrete Fourier transform.

We extend the one dimensional construction to a multidimensional context using tensor products of the points and basis functions expressed in multi-index notation. Let $\mathbf{m} = (m_1, m_2, \dots, m_d)$ represent the vector with (potentially) different number of points in each dimension, then

$$\begin{aligned} \mathbf{x}_j &= (x_{j_1}, x_{j_2}, \dots, x_{j_d}), \\ \phi_{\mathbf{j}}(\mathbf{x}) &= \prod_{k=1}^d \phi_{j_k}(x_k) = \exp\left(2\pi i \sum_{k=1}^d \sigma(j_k) \cdot x_k\right). \end{aligned}$$

The anisotropic full-tensor operator becomes:

$$\begin{aligned} \mathcal{U}^{\mathbf{m}} : C^0(\mathbb{T}^d) &\rightarrow \bigotimes_{k=1}^d \mathbb{P}_{(m_k-1)/2}, \\ \mathcal{U}^{\mathbf{m}}[f](\mathbf{x}) &= \sum_{\mathbf{j} \leq \mathbf{m}-1} \Re[\hat{c}_{\mathbf{j}} \phi_{\mathbf{j}}(\mathbf{x})]. \end{aligned}$$

As one may expect, the full-tensor interpolation coefficients are analogous to the one-dimensional case:

$$(3.5) \quad \hat{c}_{\mathbf{j}} = \frac{1}{m_1 \cdots m_d} \sum_{\mathbf{p} \leq \mathbf{m}-1} f(\mathbf{x}_{\mathbf{p}}) [\phi_{\mathbf{j}}(\mathbf{x}_{\mathbf{p}})]^*,$$

which is a normalized and re-indexed d -dimensional discrete Fourier transform.

The full-tensor construction is easy to implement, using only one-dimensional nodes and basis functions and employing a suitable algorithm for fast-Fourier transform (which is a one time computational cost). However, the resulting approximation belongs to a full-tensor space which is very far from optimal. First, we observe that the extra point incurred by the even rules in one-dimension combines with all the “good” points in other dimensions and results in a much higher penalty, e.g., in 6-dimensions the 4-point rule has 4096 points and it covers the same basis as the 3 point rule with only 729 points, thus wasting the majority of the computational effort. Restricting our attention to rules with only odd number of points, we then look at our estimate for the quasi-optimal basis. At $L = 2$, in 6 dimensions, the space has 7 exponential powers which results in 13 basis functions (all powers except zero require two basis functions), the smallest full-tensor space including $L = 2$ hyperbolic space has the aforementioned 729 points. Full-tensor interpolation is not a feasible approach in a multidimensional context.

3.2. Sparse-grid interpolation. Sparse-grid interpolation aims at exploiting the implementational simplicity of full-tensor rules while alleviating (and sometimes completely avoiding) the restrictions on the basis space. To this end, sparse-grid algorithms employ a family of one dimensional interpolation rules with different number of points and basis functions and combine (superimpose) a set of anisotropic full tensors interpolants into a single grid. The set of tensors is chosen so that the combined approximation space is as close match as possible to a desired (quasi-) optimal space.

Starting with the one-dimensional nodes and basis (3.1), we select the family of rules via the node growth $m(l)$; i.e., $m(l)$ is a strictly increasing function indicating the number of points on level $l \geq 0$. See Remark 3.2 for the specific choice used in our examples. Following the approach used in [53], we define the surplus operators

$$\Delta^{m(l)} = \mathcal{U}^{m(l)} - \mathcal{U}^{m(l-1)}, \quad \Delta^{\mathbf{m}(i)} = \bigotimes_{k=1}^d \Delta^{m(i_k)},$$

with the convention $\Delta^{m(0)} = \mathcal{U}^{m(0)}$. For any lower set $\Theta(L)$, we define the generalized interpolation operator

$$(3.6) \quad I_{\Theta(L)} = \sum_{i \in \Theta(L)} \Delta^{\mathbf{m}(i)}.$$

Our objective is to relate $\Theta(L)$ to the quasi-optimal $\Lambda(L)$, but first we observe that

$$(3.7) \quad \mathcal{U}^{\mathbf{m}(i)} = \sum_{j \leq i} \Delta^{\mathbf{m}(j)}$$

and therefore there exists a set of integer weights $\{t_i\}_{i \in \Theta(L)}$ such that

$$(3.8) \quad I_{\Theta(L)} = \sum_{i \in \Theta(L)} t_i \mathcal{U}^{\mathbf{m}(i)}.$$

By substituting (3.7) into (3.8) and equating the coefficients of the $\Delta^{\mathbf{m}(i)}$, we derive the system

$$(3.9) \quad \sum_{\substack{i \in \Theta(L) \\ j \leq i}} t_i = 1, \quad \forall j \in \Theta(L).$$

The system (3.9) can be expressed as an upper triangular matrix of zeroes and ones, with a diagonal of all ones, so a unique integer solution $\{t_i\}_{i \in \Theta(L)}$ does indeed exist.

The interpolation nodes associated with $I_{\Theta(L)}$ are the union of the nodes of all tensors $\mathcal{U}^{m(i)}$. If we want to minimize the number of nodes (and the associated expensive simulation of the target model), it is best to reuse the nodes as much as possible; i.e., we want the nodes associated with $\mathcal{U}^{m(l)}$ to be a subset of the nodes of $\mathcal{U}^{m(l+1)}$. It is well known that such nested rules are advantageous for sparse-grid methods, and thus, we restrict our attention to only those $m(l)$ that satisfy the nested property; see Remark 3.2.

Let $\Theta_m(L)$ denote the multi-indexes of the interpolation nodes for the interpolant defined by $\Theta(L)$. Then exploiting the nested structure of the rule gives

$$(3.10) \quad \Theta_m(L) = \bigcup_{i \in \Theta(L)} \{j \in \mathbb{N}^d : j \leq m(i) - 1\},$$

which comes from

$$\{\mathbf{x}_j\}_{j \in \Theta_m(L)} = \bigcup_{i \in \Theta(L)} \{\mathbf{x}_j\}_{j \leq m(i) - 1}.$$

With (3.8)-(3.10), we can explicitly write the sparse trigonometric interpolant as

$$(3.11) \quad I_{\Theta(L)}[f](\mathbf{x}) = \sum_{j \in \Theta_m(L)} \sum_{\substack{i \in \Theta(L) \\ j \leq m(i) - 1}} \Re [t_i \hat{c}_j^i \phi_j(\mathbf{x})] = \sum_{j \in \Theta_m(L)} \Re [w_j \phi_j(\mathbf{x})].$$

Here, \hat{c}_j^i and ϕ_j are defined in subsection 3.1, and

$$(3.12) \quad w_j = \sum_{\substack{i \in \Theta(L) \\ j \leq m(i) - 1}} t_i \hat{c}_j^i, \quad j \in \Theta_m(L).$$

Since each of the tensor operators exactly reproduces the basis functions, constructing $I_{\Theta(L)}[\phi_j](\mathbf{x})$ means that only non-zero coefficients will be the corresponding \hat{c}_j^i and from (3.9) follows that the interpolant is exact for all basis functions, i.e., the union of the space of all tensors. Therefore, Theorem 1 in [53] applies; since the exactness of level $l \in \mathbb{N}$ is $(m(l) - 1)/2$, then for an arbitrary lower trigonometric polynomial space $\mathbb{P}_{\Lambda(L)}$, we define the optimal sparse grid tensor set by

$$(3.13) \quad \Theta^{opt}(L) = \{i \in \mathbb{N}^d : (m(i) - 1)/2 \in \Lambda(L)\}.$$

That is, $\Theta^{opt}(L)$ is the smallest set of tensors that results in an interpolant which is exact for $\mathbb{P}_{\Lambda(L)}$. Depending on the choice of $m(l)$, the actual interpolation space may be larger.

Remark 3.2. We choose $m(l) = 3^l$, which gives us nodes that are both nested and odd-number, i.e., we avoid the cost of extra basis functions noted in Remark 3.1. The Radix-3 FFT algorithms are slightly less efficient than the Radix-2 and Radix-4 variants; however, from (3.12), we observe that the weight can be pre-computed and reused every time we need to compute the value of the interpolant. Thus, the FFT procedure is a one-time effort resulting in a small increase in computational cost, which is far offset by the reduction in interpolation nodes and model simulations. Furthermore, when targeting hyperbolic cross-section interpolation space, e.g. (2.7),

exponentially growing $m(l)$ have a natural advantage. Suppose that $\Theta(L)$ is chosen as a total degree multi-index space:

$$(3.14) \quad \Theta(L) = \left\{ \mathbf{i} \in \mathbb{N}^d : \sum_{k=1}^d \alpha_k i_k \leq L \right\} \Rightarrow \prod_{k=1}^d (3^{i_k})^{\alpha_k} \leq 3^L.$$

Then from the definition of $\Theta_m(L)$ in (3.10) and the one-to-one correspondence between nodes and basis functions, we have that the resulting space will include all ϕ_j for \mathbf{j} such that

$$\mathbf{j} + \mathbf{1} \leq \mathbf{m}(\mathbf{i}), \quad \text{i.e.} \quad j_k + 1 \leq 3^{i_k} \quad \forall 1 \leq k \leq d.$$

Combining the above with (3.14), we get the anisotropic cross-section space:

$$\prod_{k=1}^d (j_k + 1)^{\alpha_k} \leq 3^L.$$

Therefore, using an exponential $m(l)$ and total degree multi-index selection produces an interpolant in a hyperbolic cross-section space, modulo a constant in the exponent and some rounding in the actual implementation due to non-integer anisotropic rates.

3.3. Lebesgue constant. Consider the Lebesgue constant \mathbb{L}_n for $(2n+1)$ -point trigonometric interpolation. Well-known estimates for \mathbb{L}_n exist [8], including quite sharp ones [7, 44]. In terms of the Lebesgue constant, trigonometric interpolation is closely related to polynomial interpolation with the Clenshaw–Curtis and Chebyshev nodes [6, 8]. In [44], Rivlin showed the equality

$$(3.15) \quad \mathbb{L}_n = \frac{2}{\pi} \ln(n) + \beta_n, \quad n \geq 1,$$

where β_n decreases monotonically from $5/3$ to

$$\frac{2}{\pi} \left(\ln \left(\frac{16}{\pi} \right) + \gamma \right) \approx 1.404,$$

where γ is the Euler–Mascheroni constant. For our family of one dimensional rules defined by $m(l) = 3^l$, the Lebesgue constant grows as a logarithm in the number of points and linearly in level.

In general, no sharp estimates exist for the Lebesgue constant of sparse interpolation with space of exactness $\mathbb{P}_{\Lambda(L)}$. However, Lemma 3.1 in [5] yields an upper bound, i.e., when the one-dimensional rules exhibit polynomial growth in Lebesgue constant, the sparse grids constant grows no faster than polynomial with one additional power. Let $\Theta(L)$ be the optimal multi-index set corresponding to $\Lambda(L)$. Because the one-dimensional rules obey (3.15), we can bound the Lebesgue constant of the sparse interpolation operator $I_{\Theta(L)}$ in (3.11) as

$$(3.16) \quad \|I_{\Theta(L)}\| \leq C^d (\#\Theta(L))^2,$$

where $\#\Theta(L)$ is the number of multi-indexes in $\Theta(L)$. As in [5], the operator norm is defined by (2.9).

In [53], Stoyanov and Webster considered many different one-dimensional rules, some of which have Lebesgue constants that grow slowly at first but increase quite

rapidly after only a few levels. As a result, the authors included an additional parameter to account for the different “effective” Lebesgue constant in each dimension since some dimensions may have far fewer points than others. However, we do not consider such a correction in our context for the following reasons. First, the rapid increase in Lebesgue constants in [53] was not observed for the Clenshaw–Curtis nodes, which have the same linear-in-level and logarithmic-in-nodes growth as our rule. Second, the variability of β_n in (3.15) is small. Third, by using (3.15) in (2.10) and following the derivation in subsection 2.3, the Lebesgue penalty term in (2.14) is the logarithm of a logarithm, which is negligible.

3.4. Adaptive refinement. In this subsection, we will link the anisotropy least-squares problem from subsection 2.3 to the sparse trigonometric interpolation algorithm in subsection 3.2. We use (2.14), but with the sparse interpolation coefficients w_j given by (3.12), which are linear combinations of \hat{c}_j^i over the constituent tensors of the sparse grid. Also, by (3.1) and (3.4), the sparse discrete Fourier coefficient w_j corresponds to mode $\sigma(j)$. Thus, for a general lower set Λ and the corresponding Θ^{opt} , the relevant least-squares problem becomes

$$(3.17) \quad \min_{\alpha, C} \frac{1}{2} \sum_{j \in \Theta_m} (C + \alpha \cdot \bar{\sigma}(j) + \log(|w_j|))^2.$$

where Θ_m is defined by (3.10) and

$$\bar{\sigma}(j) = (\log(1 + |\sigma(j_1)|), \log(1 + |\sigma(j_2)|), \dots, \log(1 + |\sigma(j_d)|)).$$

In general, multi-index space is not easily discretizable in the sense of (2.7) after adaptive refinement takes place, so we omit dependence on L here.

We show pseudocode for our algorithm in Algorithm 3.1. Importantly, since the solution of the least-squares problem (3.17) is heavily dependent on Θ_m , then one should choose Λ_0 so that it contains enough points to compute an initial anisotropy estimate $\hat{\alpha}_0$ that is reliable (i.e., heuristically “close” to the true α). For example, if f contains only higher frequencies in some direction where only a small number of points is used, the estimate may give the appearance that the direction is not important and Algorithm 3.1 will add points in other dimensions, thus deviating significantly from the correct anisotropy of f .

Algorithm 3.1 Adaptive refinement algorithm

- 1: $n \leftarrow 0$
 - 2: Start with $\Lambda = \Lambda(L_0)$; define Θ according to (3.13)
 - 3: Compute the samples of f and load the values into the grid
 - 4: **while** num_samples < budget **do**
 - 5: Solve (3.17) for $\hat{\alpha}$
 - 6: Find L_{n+1} such that $\Lambda^{\hat{\alpha}}(L_{n+1}) \not\subseteq \Lambda$; define $\Theta^{\hat{\alpha}}(L_{n+1})$ by (3.13)
 - 7: $\Lambda \leftarrow \Lambda \cup \Lambda^{\hat{\alpha}}(L_{n+1})$; $\Theta \leftarrow \Theta \cup \Theta^{\hat{\alpha}}(L_{n+1})$; $n \leftarrow n + 1$
 - 8: Compute the samples of f at the new points
 - 9: **end while**
-

Remark 3.3. One may modify Line 6 of Algorithm 3.1 so that the number of new points is large enough to exploit parallel computations of the sample of f . When the model is sufficiently complex, parallelism must be exploited to make the problem

feasible. A possible drawback is that, if the initial grid is too coarse, [Algorithm 3.1](#) may add a large number of unnecessary nodes due to an unreliable initial anisotropy estimate.

Remark 3.4. The quasi-optimal approach aims to construct the best M -term approximation for some M given beforehand. For this reason, the termination criterion in [Line 4](#) relies on reaching some predetermined computational budget. Alternatively, if computing resources are sufficiently abundant, one could terminate upon reaching a desired error tolerance.

4. Numerical results. We include several examples in this section to illustrate the performance of [Algorithm 3.1](#). We will apply our algorithm to purpose-built periodic polynomials of known anisotropy and then to the chemistry problem that motivated this work. These simulations use the open-source Tasmanian package developed at Oak Ridge National Laboratory [50], which implements [Algorithm 3.1](#) for sparse trigonometric interpolation.

First, to obtain a theoretical convergence rate for our interpolation algorithm, let $f \in H^n(\mathbb{T})$. Using a theorem of Jackson [42], we can bound the infimum term in [\(2.10\)](#) by

$$\inf_{T \in \mathbb{P}_\Lambda} \|f - T\|_\infty \leq \frac{C}{N^{M+1}}$$

where $C > 0$ is a constant, $M = \min_k n_k$, and $N = \#\Theta_m^{opt}$ is the number of nodes. Then, using [\(3.16\)](#) and heuristically approximating $\#\Theta^{opt}$ as $\log(N)$ in light of [Remark 3.2](#),

$$(4.1) \quad \|f - I_\Theta[f]\|_\infty \leq O(\log^2(N)/N^{M+1})$$

for N sufficiently large.

Remark 4.1. (Alternative Function Space) As noted in [subsection 2.2](#), much early work on sparse grids sought to approximate function spaces of some total degree [\(2.8\)](#). In Fourier interpolation, the total-degree space is suitable for target functions f having a holomorphic extension in component k within a polyellipse of radius α_k around the real axis, for each $1 \leq k \leq d$. To see why, suppose f is a function satisfying the previous analyticity assumptions. From, e.g. [22, p. 27], the Fourier coefficients obey the sharp estimate

$$(4.2) \quad |c_j(f)| \leq C \exp(-\boldsymbol{\alpha} \cdot \mathbf{j}).$$

By taking the negative logarithm of the right-hand side of [\(4.2\)](#) and ignoring the constant, we obtain the total-degree space [\(2.8\)](#). For functions of this type, the least-squares problem [\(3.17\)](#) in [subsection 3.4](#) becomes

$$(4.3) \quad \min_{\boldsymbol{\alpha}, C} \frac{1}{2} \sum_{\mathbf{j} \in \Theta_m} (C + \boldsymbol{\alpha} \cdot |\boldsymbol{\sigma}(\mathbf{j})| + \log(|w_j|))^2,$$

where

$$|\boldsymbol{\sigma}(\mathbf{j})| = (|\sigma(j_1)|, \dots, |\sigma(j_d)|).$$

Our numerical examples will include a modification of [Algorithm 3.1](#) that uses the total-degree space [\(2.8\)](#) and the least-squares problem [\(4.3\)](#).

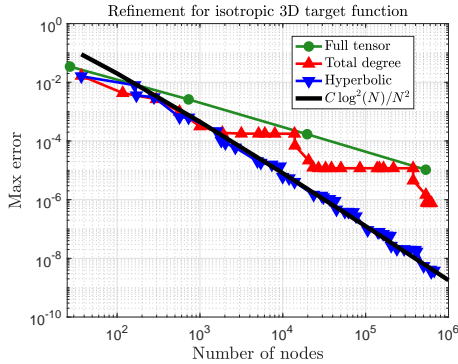


FIGURE 4.1. Isotropic refinement for trigonometric interpolation of $f_{(1,1,1)}(\mathbf{x}) = \prod_{k=1}^3 h_1(x_k)$ with different choices of $\Lambda^\alpha(L)$. Here, $\alpha = \mathbf{1}$ and refinement occurs solely by incrementing L . As expected, the hyperbolic cross-section refinement converges at the expected rate and outperforms the total-degree and full-tensor methods.

4.1. Periodic polynomials. We manufacture some multidimensional target functions that are engineered to have a certain order of differentiability and periodicity. We define the univariate functions $g_i : [-1, 1] \rightarrow \mathbb{R}$ as

$$\begin{aligned} g_1(x) &= x^3 - x, \\ g_2(x) &= \frac{x^4}{4} - \frac{x^2}{2}, \\ g_3(x) &= \frac{x^5}{20} - \frac{x^3}{6} + \frac{7}{60}x, \\ g_4(x) &= \frac{x^6}{120} - \frac{x^4}{24} + \frac{7}{120}x^2, \\ g_5(x) &= \frac{x^7}{840} - \frac{x^5}{120} + \frac{7}{360}x^2 - \frac{31}{2520}x, \end{aligned}$$

which we have derived by starting with $g_1(x)$ and integrating repeatedly, choosing the constant to preserve periodicity. By construction, $g_k \in C^k([-1, 1])$, where we interpret $[-1, 1]$ as a torus (i.e., derivatives must be continuous at the periodic boundary). For $1 \leq i \leq 5$, we normalize in the sup-norm by taking $h_i = g_i / \|g_i\|_{L^\infty([-1, 1])}$. The multivariate target functions are

$$(4.4) \quad f_i(\mathbf{x}) = \prod_{k=1}^d h_{i_k}(x_k), \quad \mathbf{1} \leq \mathbf{i} \leq \mathbf{5}.$$

The Fourier coefficients obey the estimate (2.3), so a hyperbolic function space like (2.7) is appropriate, as Figure 4.1 demonstrates. We calculate the error by drawing 2000 validation points $\mathbf{x}_j \sim \mathcal{U}(\Gamma)$, where $\mathcal{U}(\Gamma)$ is the uniform distribution on Γ , with

$$\text{error} = \max_{1 \leq j \leq 2000} |f(\mathbf{x}_j) - I_\Theta[f](\mathbf{x}_j)|.$$

In the isotropic example, the initial grids have approximately the same number of nodes, and we refine up to a maximum of 700000 nodes.

We now consider target functions with various numbers of inputs and anisotropy. The domain of interpolation is $\Gamma = [-1, 1]^d$. The initial grid for each refinement

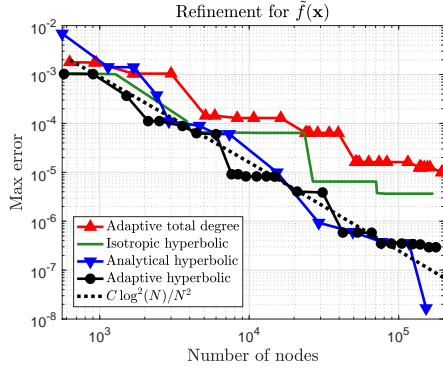


FIGURE 4.2. Convergence results for (4.5). The adaptive hyperbolic cross section methods matches the convergence rate of the analytic anisotropy, but without using any prior knowledge.

f_i	Final $\hat{\alpha}_1/\hat{\alpha}_2$ (hyperbolic)	Final $\hat{\alpha}_1/\hat{\alpha}_2$ (TD)	True α_1/α_2
(1, 2)	0.72	0.73	0.75
(1, 3)	0.61	0.61	0.60
(1, 4)	0.49	0.49	0.50
(1, 5)	0.45	0.45	0.43
(2, 3)	0.84	0.84	0.80
(2, 4)	0.68	0.68	0.67
(2, 5)	0.62	0.62	0.57
(3, 4)	0.81	0.81	0.83
(3, 5)	0.74	0.74	0.71
(4, 5)	0.91	0.91	0.86

TABLE 4.1

Anisotropy ratios for two-dimensional product functions at the end of refinement. Column 2 uses Algorithm 3.1 and Column 3 uses Remark 4.1.

strategy has approximately the same number of nodes, and we refine up to a maximum of 200000 nodes.

Next we consider an anisotropic example. In Figure 4.2, we compare different anisotropic grids, and we use the six-dimensional target function

$$(4.5) \quad \tilde{f}(\mathbf{x}) = h_1(x_1)h_5(x_4) + h_2(x_2)h_5(x_5) + h_3(x_3)h_5(x_6).$$

By construction, we know the anisotropy beforehand:

$$\boldsymbol{\alpha} = (3, 4, 5, 7, 7, 7).$$

The line labeled “Analytical hyperbolic” uses the known anisotropy $\boldsymbol{\alpha}$, while the adaptive strategies solve the relevant least-squares problem for $\hat{\boldsymbol{\alpha}}$ at each refinement iteration. In terms of convergence behavior, all strategies with a hyperbolic cross-section space outperform the total-degree space of Remark 4.1. Additionally, the adaptive algorithms based on solving the least-squares problem (3.17) converge at a similar rate as using the known target space $\Lambda^\alpha(L)$ directly. This shows that Algorithm 3.1 is well suited to handle periodic models where the anisotropy is not known a priori.

At the end of refinement, we obtain the following anisotropy estimates (normalized

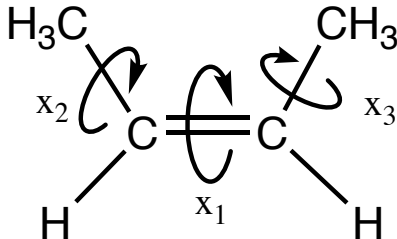


FIGURE 4.3. Molecular structure of 2-butene, labeled with rotations of interest.

so that $\hat{\alpha}_1 = \alpha_1 = 3$):

$$\begin{aligned}\hat{\alpha}_{hyp} &= (3.00, 3.53, 4.35, 5.58, 5.70, 5.73), \\ \hat{\alpha}_{TD} &= (3.00, 3.63, 4.51, 6.11, 5.73, 5.40).\end{aligned}$$

In [Table 4.1](#), we show the anisotropy ratios at the end of adaptive refinement for two-dimensional product polynomials of the form [\(4.4\)](#). We compute the true anisotropy ratio for f_i by recalling $\alpha_k = i_k + 2$. Both [Algorithm 3.1](#) and the modifications in [Remark 4.1](#) are reasonably able to detect the relative anisotropy of the target function when the initial grid yields a sufficiently accurate initial anisotropy estimate.

4.2. The 2-butene potential energy surface. Now we consider the motivating application of this paper: the adaptive approximation of a molecule’s potential energy surface (PES) where the anisotropy α is not known beforehand. The molecule of interest is 2-butene, whose molecular structure is shown in [Figure 4.3](#).

At the quantum-mechanical level, the energy \mathcal{E}_n of a molecule with an arrangement of nuclei described by \mathbf{q} satisfies the Schrödinger equation [\[29\]](#):

$$(4.6) \quad \hat{\mathcal{H}}(\mathbf{q}) \Psi_n(\mathbf{y}; \mathbf{q}) = \mathcal{E}_n(\mathbf{q}) \Psi_n(\mathbf{y}; \mathbf{q}).$$

Above, $\hat{\mathcal{H}}$ is the molecular Hamiltonian operator, \mathcal{E}_n is the energy of electronic state $n \geq 0$, and Ψ_n is the (possibly complex-valued) wavefunction of state n as a function of electron position \mathbf{y} . All terms depend parametrically on the nuclear geometry \mathbf{q} . Physically, $|\Psi_n(\mathbf{y}; \mathbf{q})|^2$ is the probability distribution function of observing an electron of energy state n at position \mathbf{y} in a molecule of geometry \mathbf{q} . As a function of geometry, $\mathcal{E}_n(\mathbf{q})$ is the PES corresponding to energy state n .

For an N -atom molecule, one may express \mathbf{q} in Cartesian coordinates as a vector with $3N$ components or in internal coordinates (bond lengths, bond angles, and torsion angles) as a vector of $3N - 6$ components. We opt for the latter, which has fewer components and directly enables the varying of geometric features. Only a few of the geometry components, denoted by \mathbf{x} (the *design variables*), may be needed in a particular study; we optimize over the rest, $\boldsymbol{\xi}$ (the *remainder variables*):

$$(4.7) \quad E_n(\mathbf{x}) = \min_{\boldsymbol{\xi}} \mathcal{E}_n(\mathbf{x}, \boldsymbol{\xi}).$$

$E_n(\mathbf{x})$ is called the *relaxed PES* for state n . Chemical intuition and knowledge of the system guides the selection of design variables. Furthermore, for rotational design variables $\boldsymbol{\theta}$, a polynomial interpolant does not guarantee periodicity of ∇E_n with respect to $\boldsymbol{\theta}$, which leads to nonphysical phenomena (e.g., nonconservation of energy).

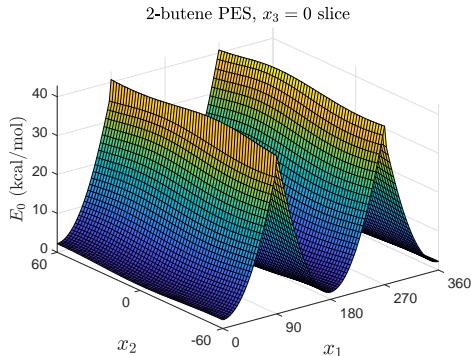


FIGURE 4.4. Slice of 2-butene PES for $x_3 = 0$.

Therefore, a trigonometric interpolation basis is appropriate when \mathbf{x} contains only bond angles and torsion angles.³

As hinted earlier, solving the optimization (4.7) subject to the generalized eigenvalue problem (4.6) is a prohibitively expensive calculation. To trim down computational cost, it is common practice in quantum chemistry to use approximate Hamiltonians and wavefunctions [29]. In our case, we use density functional theory (with the B3LYP hybrid functional) to simplify the Hamiltonian [17, 25, 47], and we approximate the wavefunctions with the 6-311G* Pople basis set [27]. We use the Gaussian 16 software package [9] to handle the approximation of Hamiltonians and wavefunctions. By default, Gaussian 16 performs the optimization in (4.7) using a variant of the EDIIS algorithm tuned for molecular geometry optimizations [30].

Previous work constructed a sparse polynomial interpolant of $E_0(\mathbf{x})$ and $E_1(\mathbf{x})$ for 2-butene to study the transition from the *cis*- to *trans*- conformation via the first singlet excited state [32]. We use the same design variables from that study, shown in Figure 4.3. The design variable x_1 is more influential on the PES than x_2 and x_3 , but the exact anisotropy is not known in advance.

The domain for our 2-butene ground-state ($n = 0$) PES is $\Gamma = [0, 360] \times [-60, 60] \times [-60, 60]$. The coordinates x_2 and x_3 correspond to dihedral rotations of CH_3 , which have period 120° . We show a slice of the 2-butene PES in Figure 4.4. Due to the ridges at $x_1 = 90$ and $x_1 = 270$, we hypothesize that the hyperbolic function space (2.7) and Algorithm 3.1 are appropriate for this problem.

There are numerous sources of noise going into the evaluation of $E_0(\mathbf{x})$: density functional theory approximates the Hamiltonian, the 6-311G* basis set approximates the wavefunction Ψ , and the optimization (4.7) has internal stopping criteria. Therefore, we do not report the max error of the interpolant $I_\Theta[E_0](\mathbf{x})$, which could be heavily skewed by non-interpolatory error. Instead, we give the root-mean-square error (RMSE) over 2000 validation points drawn uniformly over Γ :

$$(4.8) \quad \text{RMSE} = \sqrt{\frac{\sum_{j=1}^{2000} (E_0(\mathbf{x}_j) - I_\Theta[E_0](\mathbf{x}_j))^2}{2000}}, \quad \mathbf{x}_j \sim \mathcal{U}(\Gamma).$$

In our sparse grid constructions, we use Θ_{opt} based on the hyperbolic function space Λ in (2.7) as well as the total-degree space (2.8). For each variety of Θ , we refine

³Bond lengths, in general, are not periodic over an interpolation domain, so approximation by trigonometric polynomials would lead to inaccuracies at the domain boundary [16].

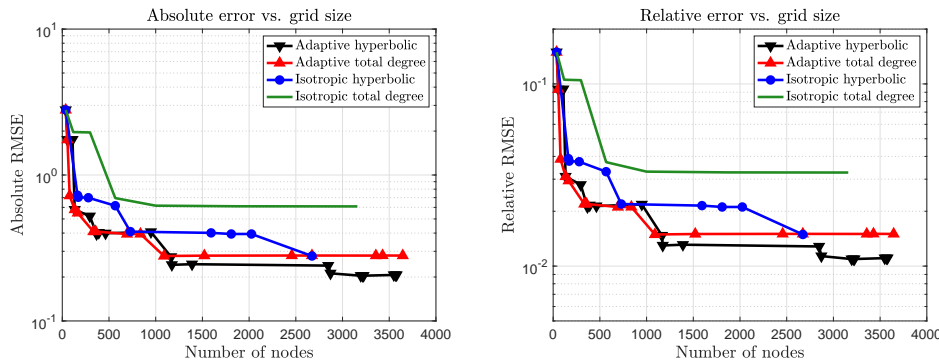


FIGURE 4.5. Absolute (left) and relative (right) error results for sparse interpolation of 2-butene ground-state PES.

both adaptively (according to [Algorithm 3.1](#) or [Remark 4.1](#)) and isotropically (taking $\alpha = 1$ and incrementing L). In all cases, we initialize each grid with 37 nodes. Since each function sample takes approximately 30 seconds to evaluate and occasionally the optimization (4.7) may fail to converge to the correct (or any) local minimum, we refine up to a maximum of only 4000 nodes. We show the results in [Figure 4.5](#). Following Pople in his 1998 Nobel lecture, we adopt 1 kcal/mol as the threshold of acceptable chemical accuracy for energies [43].

First, we note that the asymptotic absolute RMS errors in [Figure 4.5](#) are consistent with Pople’s definition of chemical accuracy for energies, and the limiting relative error for adaptive hyperbolic refinement is approximately 1%. Second, even though the one-dimensional interpolation rule (3.1) grows exponentially, we can still add smaller batches of nodes at each iteration by using (3.13) and [Algorithm 3.1](#), which mitigates the exponential growth of (3.1). Third, in both the adaptive and isotropic cases, the asymptotic error is lower for a hyperbolic cross-section than for a total-degree space.

5. Conclusion and future work. In this work, we have presented a quasi-optimal dimensionally adaptive method for sparse interpolation with a trigonometric basis. Our approach targets applications where the surrogate models must be periodicity-preserving and where the anisotropy is not known beforehand. For target functions of known finite smoothness, our algorithm matches the theoretical convergence rate, outperforms the total-degree space asymptotically, and produces a good approximation to the anisotropy. The open-source and freely available Tasmanian package contains a user-friendly implementation.

In the future, we will apply adaptive refinement to more complicated chemical systems. In particular, we aim to approximate potential energy surfaces where the geometry domain includes bond lengths, bond angles, and dihedral angles—a mix of periodic and nonperiodic inputs. To do this, we will apply trigonometric and polynomial interpolation to the periodic and nonperiodic components, respectively.

Acknowledgements. The first author was supported by an NSF Graduate Research Fellowship under DGE-1746939 and by an appointment to the Oak Ridge National Laboratory ASTRO Program, sponsored by the U.S. Department of Energy and administered by the Oak Ridge Institute for Science and Education. The second author was supported by the Exascale Computing Project (17-SC-20-SC), a

collaborative effort of the U.S. Department of Energy Office of Science and the National Nuclear Security Administration; the U.S. Defense Advanced Research Projects Agency, Defense Sciences Office under contract and award numbers HR0011619523 and 1868-A017-15; and by the Laboratory Directed Research and Development program at the Oak Ridge National Laboratory, which is operated by UT-Battelle, LLC., for the U.S. Department of Energy under Contract DE-AC05-00OR22725.

The authors also acknowledge the use of the High Performance Computing Center at North Carolina State University.

REFERENCES

- [1] V. BARTHELMANN, E. NOVAK, AND K. RITTER, *High dimensional polynomial interpolation on sparse grids*, Adv. Comput. Math., 12 (2000), pp. 273–288, <https://doi.org/10.1023/A:1018977404843>.
- [2] J. BECK, F. NOBILE, L. TAMELLINI, AND R. TEMPONE, *Convergence of quasi-optimal stochastic Galerkin methods for a class of PDEs with random coefficients*, Comput. Math. Appl., 67 (2014), pp. 732–751, <https://doi.org/10.1016/j.camwa.2013.03.004>.
- [3] R. BELLMAN, *Adaptive Control Processes: A Guided Tour*, Princeton University Press, 1961.
- [4] H.-J. BUNGARTZ AND M. GRIEBEL, *Sparse grids*, Acta Numer., 13 (2004), pp. 147–269, <https://doi.org/10.1017/S0962492904000182>.
- [5] A. CHKIFA, A. COHEN, AND C. SCHWAB, *High-dimensional adaptive sparse polynomial interpolation and applications to parametric PDEs*, Found. Comput. Math., 14 (2014), pp. 601–633, <https://doi.org/10.1007/s10208-013-9154-z>.
- [6] C. W. CLENSHAW AND A. R. CURTIS, *A method for numerical integration on an automatic computer*, Numer. Math., 2 (1960), pp. 197–205, <https://doi.org/10.1007/BF01386223>.
- [7] V. K. DZYADYK, S. Y. DZYADYK, AND A. S. PRYPIK, *Asymptotic behavior of Lebesgue constants in trigonometric interpolation*, Ukrainian Math. J., 33 (1981), pp. 553–559, <https://doi.org/10.1007/BF01085428>.
- [8] H. EHLICH AND K. ZELLER, *Auswertung der Normen von Interpolationsoperatoren*, Math. Ann., 164 (1966), pp. 105–112, <https://doi.org/10.1007/BF01429047>.
- [9] M. J. FRISCH, G. W. TRUCKS, H. B. SCHLEGEL, G. E. SCUSERIA, M. A. ROBB, J. R. CHEESEMAN, G. SCALMANI, V. BARONE, G. A. PETERSSON, H. NAKATSUJI, X. LI, M. CARICATO, A. V. MARENICH, J. BLOINO, B. G. JANESKO, R. GOMPERTS, B. MENNUCCI, H. P. HRATCHIAN, J. V. ORTIZ, A. F. IZMAYLOV, J. L. SONNENBERG, D. WILLIAMS-YOUNG, F. DING, F. LIPPARINI, F. EGIDI, J. GOINGS, B. PENG, A. PETRONE, T. HENDERSON, D. RANASINGHE, V. G. ZAKRZEWSKI, J. GAO, N. REGA, G. ZHENG, W. LIANG, M. HADA, M. EHARA, K. TOYOTA, R. FUKUDA, J. HASEGAWA, M. ISHIDA, T. NAKAJIMA, Y. HONDA, O. KITAO, H. NAKAI, T. VREVEN, K. THROSSELL, J. A. MONTGOMERY, JR., J. E. PERALTA, F. OGLIARO, M. J. BEARPARK, J. J. HEYD, E. N. BROTHERS, K. N. KUDIN, V. N. STAROVEROV, T. A. KEITH, R. KOBAYASHI, J. NORMAND, K. RAGHAVACHARI, A. P. RENDELL, J. C. BURANT, S. S. IYENGAR, J. TOMASI, M. COSSI, J. M. MILLAM, M. KLENE, C. ADAMO, R. CAMMI, J. W. OCHTERSKI, R. L. MARTIN, K. MOROKUMA, O. FARKAS, J. B. FORESMAN, AND D. J. FOX, *Gaussian 16 Revision A.03*, 2016. Gaussian Inc. Wallingford, CT.
- [10] W. GAUTSCHI, *Numerical Analysis*, Birkhäuser Basel, 2012.
- [11] L. GRAFAKOS, *Classical Fourier Analysis*, Springer, 2014.
- [12] M. GRIEBEL AND J. HAMAEEKERS, *Fast discrete Fourier transform on generalized sparse grids*, in Sparse Grids and Applications – Munich 2012, J. Garcke and D. Pflüger, eds., vol. 97 of Lecture Notes in Computational Science and Engineering, Springer International, 2014, pp. 75–107, https://doi.org/10.1007/978-3-319-04537-5_4.
- [13] M. D. GUNZBURGER, C. G. WEBSTER, AND G. ZHANG, *Stochastic finite element methods for partial differential equations with random input data*, Acta Numer., 23 (2014), pp. 521–650, <https://doi.org/10.1017/S0962492914000075>.
- [14] K. HALLATSCHKEK, *Fouriertransformation auf dünnen Gittern mit hierarchischen Basen*, Numer. Math., 63 (1992), pp. 83–97, <https://doi.org/10.1007/BF01385849>.
- [15] J. HART, A. ALEXANDERIAN, AND P. GREMAUD, *Efficient computation of Sobol’ indices for stochastic models*, SIAM J. Sci. Comput., 39 (2017), pp. A1514–A1530, <https://doi.org/10.1137/16M106193X>.
- [16] G. HELMBERG, *The Gibbs phenomenon for Fourier interpolation*, J. Approx. Theory, 78 (1994), pp. 41–63, <https://doi.org/10.1006/jath.1994.1059>.

- [17] P. HOHENBERG AND W. KOHN, *Inhomogeneous electron gas*, Phys. Rev., 136 (1964), pp. B864–B871, <https://doi.org/10.1103/PhysRev.136.B864>.
- [18] D. JACKSON, *The Theory of Approximation*, American Mathematical Society, 1930.
- [19] J. D. JAKEMAN, R. ARCHIBALD, AND D. XIU, *Characterization of discontinuities in high-dimensional stochastic problems on adaptive sparse grids*, J. Comput. Phys., 230 (2011), pp. 3977–3997, <https://doi.org/10.1016/j.jcp.2011.02.022>.
- [20] J. D. JAKEMAN, A. NARAYAN, AND D. XIU, *Minimal multi-element stochastic collocation for uncertainty quantification of discontinuous functions*, J. Comput. Phys., 242 (2013), pp. 790–808, <https://doi.org/10.1016/j.jcp.2013.02.035>.
- [21] J. D. JAKEMAN AND S. G. ROBERTS, *Local and dimension adaptive stochastic collocation for uncertainty quantification*, in Sparse Grids and Applications, Springer, 2012, pp. 181–203, https://doi.org/10.1007/978-3-642-31703-3_9.
- [22] Y. KATZNELSON, *An Introduction to Harmonic Analysis*, Cambridge University Press, 3rd ed., 2004.
- [23] V. KHAKHUTSKYY AND M. HEGLAND, *Spatially-dimension-adaptive sparse grids for online learning*, in Sparse Grids and Applications – Stuttgart 2014, Springer, 2016, pp. 133–162, https://doi.org/10.1007/978-3-319-28262-6_6.
- [24] A. KLIMKE AND B. WOHLMUTH, *Algorithm 847: spinterp: Piecewise multilinear hierarchical sparse grid interpolation in MATLAB*, ACM Trans. Math. Software, 31 (2005), pp. 561–579, <https://doi.org/10.1145/1114268.1114275>.
- [25] W. KOHN AND L. J. SHAM, *Self-consistent equations including exchange and correlation effects*, Phys. Rev., 140 (1965), pp. A1133–A1138, <https://doi.org/10.1103/PhysRev.140.A1133>.
- [26] E. KREYSZIG, *Introductory Functional Analysis with Applications*, John Wiley and Sons, 1978.
- [27] R. KRISHNAN, J. S. BINKLEY, R. SEEGER, AND J. A. POPLÉ, *Self-consistent molecular orbital methods. XX. A basis set for correlated wave functions*, J. Chem. Phys., 72 (1980), pp. 650–654, <https://doi.org/10.1063/1.438955>.
- [28] P. KRITZER, F. PILLICHSHAMMER, AND H. WOŹNIAKOWSKI, *Multivariate integration of infinitely many times differentiable functions in weighted Korobov spaces*, Math. Comp., 83 (2014), pp. 1189–1206, <https://doi.org/10.1090/S0025-5718-2013-02739-1>.
- [29] I. N. LEVINE, *Quantum Chemistry*, Pearson, 7th ed., 2014.
- [30] X. LI AND M. J. FRISCH, *Energy-represented direct inversion in the iterative subspace within a hybrid geometry optimization method*, J. Chem. Theory Comput., 2 (2006), pp. 835–839, <https://doi.org/10.1021/ct050275a>.
- [31] X. MA AND N. ZABARAS, *An adaptive hierarchical sparse grid collocation algorithm for the solution of stochastic differential equations*, J. Comput. Phys., 228 (2009), pp. 3084–3113, <https://doi.org/10.1016/j.jcp.2009.01.006>.
- [32] J. NANCE, E. JAKUBIKOVA, AND C. T. KELLEY, *Reaction path following with sparse interpolation*, J. Chem. Theory Comput., 10 (2014), pp. 2942–2949, <https://doi.org/10.1021/ct5004669>.
- [33] A. NARAYAN AND J. D. JAKEMAN, *Adaptive Leja sparse grid constructions for stochastic collocation and high-dimensional approximation*, SIAM J. Sci. Comput., 36 (2014), pp. A2952–A2983, <https://doi.org/10.1137/140966368>.
- [34] F. NOBILE, L. TAMELLINI, AND R. TEMPONE, *Convergence of quasi-optimal sparse-grid approximation of Hilbert-space-valued functions: application to random elliptic PDEs*, Numer. Math., 134 (2016), pp. 343–388, <https://doi.org/10.1007/s00211-015-0773-y>.
- [35] F. NOBILE, R. TEMPONE, AND C. G. WEBSTER, *An anisotropic sparse grid stochastic collocation method for partial differential equations with random input data*, SIAM J. Numer. Anal., 46 (2008), pp. 2411–2442, <https://doi.org/10.1137/070680540>.
- [36] E. NOVAK AND K. RITTER, *High dimensional integration of smooth functions over cubes*, Numer. Math., 75 (1996), pp. 79–97, <https://doi.org/10.1007/s002110050231>.
- [37] E. NOVAK AND K. RITTER, *Simple cubature formulas with high polynomial exactness*, Constr. Approx., 15 (1999), pp. 499–522, <https://doi.org/10.1007/s003659900119>.
- [38] E. NOVAK AND H. WOŹNIAKOWSKI, *Tractability of Multivariate Problems*, European Mathematical Society, 2008.
- [39] A. PAPAGEORGIOU AND H. WOŹNIAKOWSKI, *Tractability through increasing smoothness*, J. Complexity, 26 (2010), pp. 409–421, <https://doi.org/10.1016/j.jco.2009.12.004>.
- [40] D. PFLÜGER, *Spatially adaptive refinement*, in Sparse Grids and Applications, Springer, 2012, pp. 243–262, https://doi.org/10.1007/978-3-642-31703-3_12.
- [41] D. PFLÜGER, B. PEHERSTORFER, AND H.-J. BUNGARTZ, *Spatially adaptive sparse grids for high-dimensional data-driven problems*, J. Complexity, 26 (2010), pp. 508–522, <https://doi.org/10.1016/j.jco.2010.04.001>.

- [42] A. PINKUS, *Negative theorems in approximation theory*, Amer. Math. Monthly, 110 (2003), pp. 900–911, <https://doi.org/10.1080/00029890.2003.11920030>.
- [43] J. A. POPLE, *Nobel lecture: Quantum chemical models*, Rev. Mod. Phys., 71 (1999), pp. 1267–1274, <https://doi.org/10.1103/RevModPhys.71.1267>.
- [44] T. J. RIVLIN, *The Chebyshev Polynomials*, Wiley, 1st ed., 1974.
- [45] W. SICKEL AND T. ULLRICH, *Tensor products of Sobolev–Besov spaces and applications to approximation from the hyperbolic cross*, J. Approx. Theory, 161 (2009), pp. 748–786, <https://doi.org/10.1016/j.jat.2009.01.001>.
- [46] S. A. SMOLYAK, *Quadrature and interpolation formulas for tensor products of certain classes of functions*, Dokl. Akad. Nauk SSSR, 148 (1963), pp. 1042–1045.
- [47] P. J. STEPHENS, F. J. DEVLIN, C. F. CHABALOWSKI, AND M. J. FRISCH, *Ab initio calculation of vibrational absorption and circular dichroism spectra using density functional force fields*, J. Phys. Chem., 98 (1994), pp. 11623–11627, <https://doi.org/10.1021/j100096a001>.
- [48] J. STOER AND R. BULIRSCH, *Introduction to Numerical Analysis*, Springer-Verlag, 2nd ed., 1993. Translated from German by R. Bartels, W. Gautschi, and C. Witzgall.
- [49] M. STOYANOV, *Adaptive sparse grid construction in a context of local anisotropy and multiple hierarchical parents*, in Sparse Grids and Applications – Miami 2016, Springer, 2018, pp. 175–199, https://doi.org/10.1007/978-3-319-75426-0_8.
- [50] M. STOYANOV, *TASMANIAN sparse grids (version 6.0)*, Tech. Report ORNL/TM-2015/596, Oak Ridge National Laboratory, 2018, <https://tasmanian.ornl.gov/>.
- [51] M. STOYANOV, P. SELESON, AND C. WEBSTER, *Predicting fracture patterns in simulations of brittle materials under variable load and material strength*, in 19th AIAA Non-Deterministic Approaches Conference, 2017, p. 1326, <https://doi.org/10.2514/6.2017-1326>.
- [52] M. STOYANOV AND C. G. WEBSTER, *A gradient-based sampling approach for dimension reduction of partial differential equations with stochastic coefficients*, Int. J. Uncertain. Quantif., 5 (2015), pp. 49–72, <https://doi.org/10.1615/Int.J.UncertaintyQuantification.2014010945>.
- [53] M. K. STOYANOV AND C. G. WEBSTER, *A dynamically adaptive sparse grids method for quasi-optimal interpolation of multidimensional functions*, Comput. Math. Appl., 71 (2016), pp. 2449–2465, <https://doi.org/10.1016/j.camwa.2015.12.045>.
- [54] R. A. TODOR AND C. SCHWAB, *Convergence rates for sparse chaos approximations of elliptic problems with stochastic coefficients*, IMA J. Numer. Anal., 27 (2007), pp. 232–261, <https://doi.org/10.1093/imanum/drl025>.
- [55] H. TRAN, C. G. WEBSTER, AND G. ZHANG, *Analysis of quasi-optimal polynomial approximations for parameterized PDEs with deterministic and stochastic coefficients*, Numer. Math., 137 (2017), pp. 451–493, <https://doi.org/10.1007/s00211-017-0878-6>.